Control Authority of a Projectile Equipped with a Controllable Internal Translating Mass

Jonathan Rogers[*] and Mark Costello[†]

Georgia Institute of Technology, Atlanta, Georgia 30332

A physical method to alter the trajectory of a projectile is a critical element of any smart weapon. Creation of an appropriate control mechanism is often one of the more difficult parts of the overall design due to size, durability, and control authority requirements. The work reported here considers a vibrating internal mass control mechanism applicable to both fin- and spin-stabilized configurations. To investigate the potential of this control mechanism, a 7-degree-of-freedom flight dynamic model of a projectile equipped with an internal translating mass is generated. By vibrating the internal translating mass normal to the axis of symmetry and at the roll rate frequency, significant control authority can be attained with a relatively small internal mass on the order of a percent or so of the total projectile mass. Interestingly, control authority increases proportionally with increasing roll rate and also with increasing station-line cavity offset from the mass center. Trajectory changes are not caused by lateral mass center offset and drag but rather by dynamic coupling between internal mass vibration and the projectile body.

Nomenclature

A_T	=	internal translating mass oscillation amplitude
$\boldsymbol{a}_{C/I}$	=	translational acceleration vector of the system center of mass with respect to the inertial frame
$\boldsymbol{a}_{P/I}$	=	translational acceleration of the projectile center of mass with respect to the inertial frame
$\boldsymbol{a}_{T/I}$	=	translational acceleration vector of the internal translating mass center of mass with respect to the inertial frame
$\boldsymbol{a}_{T/P}$	=	translational acceleration of the internal translating mass with respect to the projectile reference frame
B	=	point at center of internal translating mass cavity
C	=	point at center of mass of composite projectile-translating mass system
C_i	=	various projectile aerodynamic coefficients
c_V	=	viscous damping coefficient in the sleeve for the internal translating mass
D	=	projectile reference diameter
$\boldsymbol{F}_C$	=	constraint force on the internal translating mass
$\boldsymbol{F}_F$	=	frictional force exerted on the internal translating mass by the cavity wall
$\boldsymbol{F}_I$	=	input force exerted by controller along translating mass line of movement
$\boldsymbol{F}_P$	=	total aerodynamic force exerted on the projectile
f_{input}	=	scalar value of the input force exerted by the controller
g	=	acceleration due to gravity (9.81 m/s²)
$\boldsymbol{H}_{P/I}$	=	angular momentum of the projectile with respect to the inertial frame about the projectile body mass center
$\boldsymbol{H}_{T/I}$	=	angular momentum of the internal translating mass with respect to the inertial frame about the internal translating mass center
$\boldsymbol{I}_I, \boldsymbol{J}_I, \boldsymbol{K}_I$	=	inertial reference frame unit vectors
$\boldsymbol{I}_{NR}, \boldsymbol{J}_{NR}, \boldsymbol{K}_{NR}$	=	no roll reference frame unit vectors
I_P	=	mass moment of inertia matrix of the projectile body with respect to the projectile reference frame
$\boldsymbol{I}_P, \boldsymbol{J}_P, \boldsymbol{K}_P$	=	projectile reference frame unit vectors
I_T	=	mass moment of inertia matrix of the internal translating mass with respect to the projectile reference frame
$\boldsymbol{I}_T, \boldsymbol{J}_T, \boldsymbol{K}_T$	=	internal translating mass reference frame unit vectors
L, M, N	=	external moment components on the projectile body expressed in the projectile reference frame
L_B	=	length of projectile
M_{JNR}	=	average moment exerted on the composite body in the $\boldsymbol{J}_{NR}$ direction
M_{KNR}	=	average moment exerted on the composite body in the $\boldsymbol{K}_{NR}$ direction
$\boldsymbol{M}^C$	=	total external moment applied to the system about the system mass center
m	=	total system mass
m_P	=	projectile body mass
m_T	=	internal translating mass
P	=	point at mass center of projectile with cavity
p, q, r	=	components of the angular velocity vector of the projectile body expressed in the projectile reference frame
$\tilde{p}, \tilde{q}, \tilde{r}$	=	components of the angular velocity vector of the projectile body expressed in the no roll reference frame
q_a	=	dynamic pressure at the projectile mass center
$\boldsymbol{r}_{C \to P}$	=	distance vector from the center of mass of the system to the projectile center of mass
$\boldsymbol{r}_{C \to T}$	=	distance vector from the center of mass of the system to the internal translating mass center of mass
$\boldsymbol{r}_{P \to T}$	=	distance vector from the projectile center of mass to the internal translating mass center of mass
r_{PA}	=	cavity offset from the projectile center of mass

*Graduate Research Assistant, School of Aeronautical Engineering. Member AIAA.

†Sikorsky Associate Professor, School of Aerospace Engineering. Associate Fellow AIAA.

s	=	location of the internal translating mass along its line of movement
$s_{command}$	=	commanded position of the internal translating mass by the controller
T_{IP}	=	transformation matrix from the inertial reference frame to the projectile reference frame
T_{NRP}	=	transformation matrix from the projectile reference frame to the no roll reference frame
T_{PT}	=	transformation matrix from the projectile reference frame to the internal translating mass reference frame
u, v, w	=	translation velocity components of the composite body center of mass resolved in the projectile reference frame
V	=	magnitude of mass center velocity
$\boldsymbol{v}_{C/I}$	=	velocity of the system mass center with respect to the inertial frame
v_S	=	magnitude of the velocity of the translating mass with respect to the translating mass reference frame
$\boldsymbol{v}_{T/P}$	=	velocity of the internal translating mass center of mass with respect to the projectile reference frame
W_P	=	weight of the projectile (without the internal mass)
W_T	=	weight of the internal translating mass
X, Y, Z	=	total external force components on the composite body expressed in the fixed plane reference frame
X_T	=	distance from the center of the internal translating mass cavity to the system center of mass
x, y, z	=	position vector components of the composite body center of mass expressed in the inertial reference frame
α	=	longitudinal aerodynamic angle of attack
$\boldsymbol{\alpha}_{P/I}$	=	angular acceleration of the projectile body with respect to the inertial frame
β	=	lateral aerodynamic angle of attack
Δy_S	=	swerve measured in the $\boldsymbol{J}_I$ direction
Δz_S	=	swerve measured in the $\boldsymbol{K}_I$ direction
θ_T, ψ_T	=	Euler pitch and yaw angles for the orientation of the line of movement of the internal translating mass with respect to the projectile body
ξ	=	damping ratio of the feedback linearization controller
ρ	=	density of air
Φ_T	=	phase angle of projectile swerve at impact
ϕ, θ, ψ	=	Euler roll, pitch, and yaw angles
ϕ_T	=	phase angle of controller input with respect to Euler roll angle
ω_N	=	natural frequency of the feedback linearization controller
$\boldsymbol{\omega}_{P/I}$	=	angular velocity of the projectile body with respect to the inertial frame

I.   Introduction

BECAUSE of the convergence of rugged and small sensors with equally rugged and small powerful microprocessors, projectiles are now being designed with full guidance and control capability. A key component of new guided projectiles is the control mechanism. The control mechanism must be capable of altering the trajectory of the projectile in such a way that impact point errors induced at launch and in flight can be corrected. At the same time, the control mechanism must be rugged to withstand high acceleration loads at launch, small so that payload space is not compromised, and

inexpensive for cost considerations. There are many different control mechanisms being developed with these requirements in mind, but all concepts essentially fall into three categories: aerodynamic load mechanisms, jet thrust mechanisms, and inertial load mechanisms. Examples of aerodynamic control mechanisms include rotation of aerodynamic lifting surface appendages, deflection of the nose, and deflection of ram air to side ports. Examples of jet thrust control mechanisms include gas jet thrusters and explosive thrusters. Examples of inertial control mechanisms include internal translation of a control mass and internal rotation of an unbalanced part. Many conventional uncontrolled projectile configurations contain internal parts that move slightly in flight such as, for example, submunitions keyed into place and ball rotor fuses on some indirect fire shells. These moving internal parts are known to cause significant alterations in the trajectory of the round. Although seemingly insignificant from a dynamic modeling perspective, small mass unbalances in these configurations can induce instability of the round as a whole typified in flight by a large loss in range and large spin decay. These observations motivated several investigators to consider dynamic stability of projectiles with moving internal components [1]. Soper [2] evaluated the stability of a spinning projectile that contains a cylindrical mass fitted loosely into a cylindrical cavity. Using a similar geometric configuration, Murphy [3] developed a quasi-linear solution for a projectile with an internal moving part. Later, D'Amico [4] performed a detailed series of experiments where a projectile with a loose internal part was driven by the rotor of a freely gimbaled gyroscope. Hodapp [5] expanded the work of Soper [2] and Murphy [3] by considering a projectile configuration with a partially restrained internal member with a mass center offset.

The basic idea of using moveable internal components as a control mechanism has been considered for different air vehicle configurations by several investigators. Petsopoulos et al. [6] considered employment of a moving mass inside a reentry vehicle to create a means for roll control. Robinett et al. [7] used internally moving masses in a plane normal to the axis of symmetry of ballistic rockets to achieve control while more recently Menon et al. [8] considered exoatmospheric interception scenarios using three orthogonal internal translating masses as the control mechanism. An active control system was developed using a feedback linearization technique. Frost and Costello [9,10] investigated the ability of an internal rotating mass unbalance to actively control both fin and spin-stabilized projectiles.

The work reported here seeks to harness trajectory alteration potential of a single vibrating internally translating part aligned in the lateral direction. This paper begins with a description of a 7-degrees of freedom flight dynamic model used for trajectory predictions along with a description of a flight control system to generate control authority. The dynamic model is subsequently employed to predict control authority as well as actuator power requirements for an example projectile. The effects of key physical properties of the system such as internal mass ratio, spin rate, cavity station-line location, and aerodynamic properties are examined against swerve production capability versus actuator power required.

II.   Internal Translating Mass Projectile Dynamic Model

A sketch of the basic projectile configuration is shown in Fig. 1. It consists of two major components, namely, a main projectile body and an internal translating mass. The main projectile body is largely a typical projectile with the exception of an internal cavity that hosts an internal mass. The internal mass is free to translate within the main projectile cavity. An actuator inside the projectile exerts a force on the internal mass as well as the main projectile to move the mass inside the cavity to a desired location.

Four reference frames are used in development of the equations of motion for the system, namely, the inertial, projectile, no roll, and translating mass reference frames. The four reference frames are linked by the following three orthonormal transformation matrices:
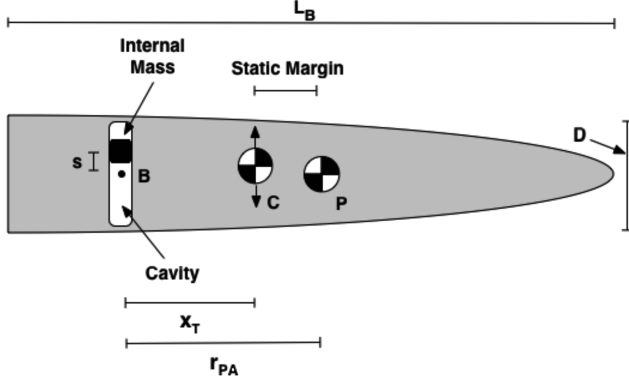
C: The mass center of the composite projectile-internal moving mass system.
P: The mass center of the projectile with the cavity.
B: The center of the internal translating mass cavity.

Fig. 1 The internal moving mass projectile. The cavity is located behind the mass center of the composite system, and the line of movement is along the hollow cavity as shown.

$$
\begin{Bmatrix} I_P \\ J_P \\ K_P \end{Bmatrix} =
\begin{bmatrix}
c_\theta c_\psi & c_\theta s_\psi & -s_\theta \\
s_\phi s_\theta c_\psi - c_\phi s_\psi & s_\phi s_\theta s_\psi + c_\phi c_\psi & s_\phi c_\theta \\
c_\phi s_\theta c_\psi + s_\phi s_\psi & c_\phi s_\theta s_\psi - s_\phi c_\psi & c_\phi c_\theta
\end{bmatrix}
\begin{Bmatrix} I_I \\ J_I \\ K_I \end{Bmatrix}
$$

$$
= [T_{IP}] \begin{Bmatrix} I_I \\ J_I \\ K_I \end{Bmatrix} \tag{1}
$$

$$
\begin{Bmatrix} I_T \\ J_T \\ K_T \end{Bmatrix} =
\begin{bmatrix}
c_{\theta_T} c_{\psi_T} & c_{\theta_T} s_{\psi_T} & -s_{\theta_T} \\
-s_{\psi_T} & c_{\psi_T} & 0 \\
s_{\theta_T} c_{\psi_T} & s_{\theta_T} s_{\psi_T} & c_{\theta_T}
\end{bmatrix}
\begin{Bmatrix} I_P \\ J_P \\ K_P \end{Bmatrix}
= [T_{PT}] \begin{Bmatrix} I_P \\ J_P \\ K_P \end{Bmatrix} \tag{2}
$$

$$
\begin{Bmatrix} I_{NR} \\ J_{NR} \\ K_{NR} \end{Bmatrix} =
\begin{bmatrix}
1 & 0 & 0 \\
0 & c_\phi & -s_\phi \\
0 & s_\phi & c_\phi
\end{bmatrix}
\begin{Bmatrix} I_P \\ J_P \\ K_P \end{Bmatrix}
= [T_{NRP}] \begin{Bmatrix} I_P \\ J_P \\ K_P \end{Bmatrix} \tag{3}
$$

The T frame is assumed to be fixed with respect to the P frame, and therefore the angles ψ_T and θ_T do not change with time. All equations in this paper use the following shorthand notation for trigonometric sine, cosine, and tangent functions: $s_\alpha = \sin\alpha$, $c_\alpha = \cos\alpha$, and $t_\alpha = \tan\alpha$.

Throughout the development of the equations of motion, several different position vectors are used. The nomenclature for position vectors is such that $r_{\alpha \to \beta}$ is defined as the position vector from point α to point β. The position vector of the mass center of the two-body system with respect to a ground fixed reference frame is written as

$$
r_{O \to C} = x I_I + y J_I + z K_I \tag{4}
$$

whereas the position of the internal translating mass with respect to the projectile reference frame is

$$
r_{C \to T} = (x_T + s(c_{\theta_T} c_{\psi_T})) I_P + (s(c_{\theta_T} s_{\psi_T})) J_P + (s(-s_{\theta_T})) K_P \tag{5}
$$

The mathematical model describing the motion of the internal translating mass projectile allows for four translational and three rotational rigid body degrees of freedom. The translation degrees of freedom are the three components of the composite body mass center position vector (x, y, z) and the position of the internal translating mass with respect to the projectile body (s). The rotation degrees of freedom are the Euler roll, pitch, and yaw angles (ϕ, θ, ψ) mentioned previously.

The vector component operator shown in Eq. (5) outputs a column vector composed of the components of an input vector in a given frame. For example, if the position vector from α to β is expressed in reference frame A as $r_{\alpha \to \beta} = \Delta x_{\alpha\beta} I_A + \Delta y_{\alpha\beta} J_A + \Delta z_{\alpha\beta} K_A$ then the vector component operator acting on this vector yields

$$
\mathbb{C}_A(r_{\alpha \to \beta}) = \begin{Bmatrix} \Delta x_{\alpha\beta} \\ \Delta y_{\alpha\beta} \\ \Delta z_{\alpha\beta} \end{Bmatrix} \tag{6}
$$

Notice that the reference frame is denoted by the subscript on the operator.

The cross-product operator outputs a skew symmetric matrix using the components of an input vector in the reference frame denoted in the subscript. For example, if the position vector from α to β is expressed in reference frame A as $r_{\alpha \to \beta} = \Delta x_{\alpha\beta} I_A + \Delta y_{\alpha\beta} J_A + \Delta z_{\alpha\beta} K_A$ then the cross-product operator acting on $r_{\alpha \to \beta}$ expressed in reference frame A is

$$
\mathbb{S}_A(r_{\alpha \to \beta}) = \begin{bmatrix}
0 & -\Delta z_{\alpha\beta} & \Delta y_{\alpha\beta} \\
\Delta z_{\alpha\beta} & 0 & -\Delta x_{\alpha\beta} \\
-\Delta y_{\alpha\beta} & \Delta x_{\alpha\beta} & 0
\end{bmatrix} \tag{7}
$$

A. Kinematics

The velocity of the composite body mass center can be described in the inertial frame or the projectile reference frame:

$$
v_{C/I} = \dot{x} I_I + \dot{y} J_I + \dot{z} K_I = u I_P + v J_P + w K_P \tag{8}
$$

The translational kinematic differential equations relate these two representations of the mass center velocity components:

$$
\begin{Bmatrix} \dot{x} \\ \dot{y} \\ \dot{z} \end{Bmatrix} =
\begin{bmatrix}
c_\theta c_\psi & s_\phi s_\theta c_\psi - c_\phi s_\psi & c_\phi s_\theta c_\psi + s_\phi s_\psi \\
c_\theta s_\psi & s_\phi s_\theta s_\psi + c_\phi c_\psi & c_\phi s_\theta s_\psi - s_\phi c_\psi \\
-s_\theta & s_\phi c_\theta & c_\phi c_\theta
\end{bmatrix}
\begin{Bmatrix} u \\ v \\ w \end{Bmatrix}
$$

$$
= [T_{IP}]^T \begin{Bmatrix} u \\ v \\ w \end{Bmatrix} \tag{9}
$$

The angular velocity of the projectile with respect to the inertial reference frame can be written in terms of appropriate Euler angle time derivatives or in terms of projectile frame angular velocity components:

$$
\omega_{P/I} = \dot{\phi} I_P + \dot{\theta} J_N + \dot{\psi} K_I = p I_P + q J_P + r K_p \tag{10}
$$

The kinematic relationship between time derivatives of the Euler angles and projectile reference frame angular velocity components represents the rotational kinematic differential equations:

$$
\begin{Bmatrix} \dot{\phi} \\ \dot{\theta} \\ \dot{\psi} \end{Bmatrix} =
\begin{bmatrix}
1 & s_\phi t_\theta & c_\phi t_\theta \\
0 & c_\phi & -s_\phi \\
0 & s_\phi/c_\theta & c_\phi/c_\theta
\end{bmatrix}
\begin{Bmatrix} p \\ q \\ r \end{Bmatrix} \tag{11}
$$

The final kinematic differential equation is the trivial relationship

$$
\dot{s} = v_S \tag{12}
$$

B. Dynamics

The translational dynamic equations for both the projectile and internal mass are derived through force balancing. They are given by

$$
m_p a_{P/I} = W_P + F_P - F_C - F_I - F_F \tag{13}
$$

$$
m_T a_{T/I} = W_T + F_C + F_I + F_F \tag{14}
$$

Also note that the definition of the center of mass of a the system leads to

$$m\boldsymbol{a}_{C/I} = m_P\boldsymbol{a}_{P/I} + m_T\boldsymbol{a}_{T/I} \qquad (15)$$

By adding Eqs. (13) and (14) and noting the mass center definition in Eq. (15), the translational dynamics equation for the system is formed,

$$m\boldsymbol{a}_{C/I} = \boldsymbol{W}_P + \boldsymbol{W}_T + \boldsymbol{F}_P \qquad (16)$$

Writing Eq. (15) in the projectile reference frame yields

$$\begin{Bmatrix} \dot{u} \\ \dot{v} \\ \dot{w} \end{Bmatrix} = \begin{Bmatrix} \frac{X}{m} \\ \frac{Y}{m} \\ \frac{Z}{m} \end{Bmatrix} - \begin{bmatrix} 0 & -r & q \\ r & 0 & -p \\ -q & p & 0 \end{bmatrix} \begin{Bmatrix} u \\ v \\ w \end{Bmatrix} \qquad (17)$$

Another translational dynamic equation is formed from the $\boldsymbol{I}_T$ component of the translating mass equation of motion shown in Eq. (13). The well-known formula for one point moving on a rigid body yields [9]

$$\boldsymbol{a}_{T/I} = \boldsymbol{a}_{P/I} + \boldsymbol{a}_{T/P} + (\boldsymbol{\alpha}_{P/I} \times \boldsymbol{r}_{P\rightarrow T}) + 2(\boldsymbol{\omega}_{P/I} \times \boldsymbol{v}_{T/P})$$
$$+ (\boldsymbol{\omega}_{P/I} \times (\boldsymbol{\omega}_{P/I} \times \boldsymbol{r}_{P\rightarrow T})) \qquad (18)$$

The mass center definition allows a substitution for $\boldsymbol{a}_{P/I}$, yielding

$$\boldsymbol{a}_{T/I} = \boldsymbol{a}_{C/I} + \frac{m_P}{m}[\boldsymbol{a}_{T/P} + (\boldsymbol{\alpha}_{P/I} \times \boldsymbol{r}_{P\rightarrow T}) + 2(\boldsymbol{\omega}_{P/I} \times \boldsymbol{v}_{T/P})$$
$$+ (\boldsymbol{\omega}_{P/I} \times (\boldsymbol{\omega}_{P/I} \times \boldsymbol{r}_{P\rightarrow T}))] \qquad (19)$$

Multiplying through by m_T,

$$m_T\boldsymbol{a}_{T/I} = m_T\boldsymbol{a}_{C/I} + \frac{m_Pm_T}{m}[\boldsymbol{a}_{T/P} + (\boldsymbol{\alpha}_{P/I} \times \boldsymbol{r}_{P\rightarrow T})$$
$$+ 2(\boldsymbol{\omega}_{P/I} \times \boldsymbol{v}_{T/P}) + (\boldsymbol{\omega}_{P/I} \times (\boldsymbol{\omega}_{P/I} \times \boldsymbol{r}_{P\rightarrow T}))] \qquad (20)$$

Notice also that the constraint force along $\boldsymbol{I}_T$ is zero because motion along this axis is permitted in the model. The translating mass equation of motion is therefore

$$m_T\boldsymbol{a}_{C/I} + \frac{m_Pm_T}{m}[\boldsymbol{a}_{T/P} + (\boldsymbol{\alpha}_{P/I} \times \boldsymbol{r}_{P\rightarrow T}) + 2(\boldsymbol{\omega}_{P/I} \times \boldsymbol{v}_{T/P})$$
$$+ (\boldsymbol{\omega}_{P/I} \times (\boldsymbol{\omega}_{P/I} \times \boldsymbol{r}_{P\rightarrow T}))] = \boldsymbol{W}_T + \boldsymbol{F}_C + \boldsymbol{F}_I + \boldsymbol{F}_F \qquad (21)$$

Extracting the $\boldsymbol{I}_T$ component of this equation is accomplished by taking the inner product of the equation with $\boldsymbol{I}_T$. Notice the following simplifications:

$$\boldsymbol{I}_T \cdot \boldsymbol{F}_C = 0 \qquad (22)$$

$$\boldsymbol{I}_T \cdot (\boldsymbol{\omega}_{P/I} \times \boldsymbol{v}_{T/P}) = 0 \qquad (23)$$

$$\boldsymbol{I}_T \cdot \boldsymbol{a}_{T/P} = \ddot{s} \qquad (24)$$

$$\boldsymbol{I}_T \cdot \boldsymbol{F}_I = f_{\text{input}} \qquad (25)$$

$$\boldsymbol{I}_T \cdot \boldsymbol{F}_F = -c_V\dot{s} \qquad (26)$$

In component form, this equation of motion is written as

$$[A_{S1} \quad A_{S2} \quad A_{S3}]\begin{Bmatrix} \dot{u} \\ \dot{v} \\ \dot{w} \\ \ddot{s} \\ \dot{p} \\ \dot{q} \\ \dot{r} \end{Bmatrix} = \{B_S\} \qquad (27)$$

where

$$A_{S1} = m_T[c_{\theta_T}c_{\psi_T}, c_{\theta_T}s_{\psi_T}, -s_{\theta_T}] \qquad (28)$$

$$A_{S2} = \frac{m_Pm_T}{m} \qquad (29)$$

$$A_{S3} = -\frac{m_Pm_T}{m}[c_{\theta_T}c_{\psi_T}, c_{\theta_T}s_{\psi_T}, -s_{\theta_T}]\mathbb{S}_P(\boldsymbol{r}_{P\rightarrow T}) \qquad (30)$$

$$B_S = f_{\text{input}} - c_V\dot{s} + m_Tg(-s_\theta c_{\theta_T}c_{\psi_T} + s_\phi c_\theta c_{\theta_T}s_{\psi_T} - c_\phi c_\theta s_{\theta_T})$$
$$- m_T[c_{\theta_T}c_{\psi_T}, c_{\theta_T}s_{\psi_T}, -s_{\theta_T}]\mathbb{S}_P(\boldsymbol{\omega}_{P/I})\mathbb{C}_P(\boldsymbol{v}_{C/I})$$
$$- \frac{m_Pm_T}{m}[c_{\theta_T}c_{\psi_T}, c_{\theta_T}s_{\psi_T}, -s_{\theta_T}]\mathbb{S}_P(\boldsymbol{\omega}_{P/I})\mathbb{S}_P(\boldsymbol{\omega}_{P/I})\mathbb{C}_P(\boldsymbol{r}_{P\rightarrow T})$$
$$\qquad (31)$$

The rotation kinetic differential equations are obtained by equating the $\boldsymbol{I}$ frame time rate of change of the system angular momentum about the system mass center to the total applied external moments to the system about the system mass center,

$$\frac{{}^I\mathrm{d}\boldsymbol{H}^P_{P/I}}{\mathrm{d}t} + \frac{{}^I\mathrm{d}\boldsymbol{H}^T_{T/I}}{\mathrm{d}t} + m_P\boldsymbol{r}_{C\rightarrow P} \times \boldsymbol{a}_{P/I} + m_T\boldsymbol{r}_{C\rightarrow T} \times \boldsymbol{a}_{T/I} = \boldsymbol{M}^C \qquad (32)$$

Expressed in the projectile reference frame, the components of this equation are

$$A_{RR}\begin{Bmatrix} \dot{p} \\ \dot{q} \\ \dot{r} \end{Bmatrix} + A_{RS}\{\ddot{s}\} = \{B_R\} \qquad (33)$$

where

$$A_{RR} = I_P + I_T - \frac{m_T}{m_P}m\mathbb{S}_P(r_{C\rightarrow T})\mathbb{S}_P(r_{C\rightarrow T}) \qquad (34)$$

$$A_{RS} = m_T\mathbb{S}_P(r_{C\rightarrow T})[T_{PT}]^T \qquad (35)$$

$$B_R = \begin{Bmatrix} M_X \\ M_Y \\ M_Z \end{Bmatrix} - \mathbb{S}_P(\boldsymbol{\omega}_{P/I})\left(I_P + I_T - \frac{m_T}{m_P}m\mathbb{S}_P(r_{C\rightarrow T})\mathbb{S}_P(r_{C\rightarrow T})\right)$$
$$\times \mathbb{C}_P(\boldsymbol{\omega}_{P/I}) - 2m_T\mathbb{S}_P(r_{C\rightarrow T})\mathbb{S}_P(\boldsymbol{\omega}_{P/I})[T_{PT}]^T\begin{Bmatrix} \dot{s} \\ 0 \\ 0 \end{Bmatrix} \qquad (36)$$

The dynamic equations of motion for the internal translating mass projectile are collectively given by Eqs. (9), (11), (12), (27), and (33). With a known set of initial conditions for the projectile, these 14 scalar equations are numerically integrated forward in time using a fourth-order Runge–Kutta algorithm to obtain a single trajectory.

C. Projectile Applied Forces and Moments

In the equations developed above, applied loads drive the motion of the projectile. The total applied force on the system is given by

$$\begin{Bmatrix} X \\ Y \\ Z \end{Bmatrix} = \begin{Bmatrix} X_P \\ Y_P \\ Z_P \end{Bmatrix} + \begin{Bmatrix} X_T \\ Y_T \\ Z_T \end{Bmatrix} \tag{37}$$

Only expressions for the applied loads on the projectile are shown. The weight force on the translating mass is similar to the projectile with obvious changes:

$$\begin{Bmatrix} X_P \\ Y_P \\ Z_P \end{Bmatrix} = \begin{Bmatrix} X_P^W \\ Y_P^W \\ Z_P^W \end{Bmatrix} + \begin{Bmatrix} X_P^A \\ Y_P^A \\ Z_P^A \end{Bmatrix} + \begin{Bmatrix} X_P^I \\ Y_P^I \\ Z_P^I \end{Bmatrix} \tag{38}$$

$$\begin{Bmatrix} L_P \\ M_P \\ N_P \end{Bmatrix} = \begin{Bmatrix} L_P^A \\ M_P^A \\ N_P^A \end{Bmatrix} + \begin{Bmatrix} L_P^I \\ M_P^I \\ N_P^I \end{Bmatrix} \tag{39}$$

The next several sections detail the different terms in the above equation. The control forces and moments are computed within the control system, which is described later, hence expressions are not provided here.

1. Weight Force

The projectile weight force expressed in the projectile frame is

$$\begin{Bmatrix} X_P^W \\ Y_P^W \\ Z_P^W \end{Bmatrix} = m_P g \begin{Bmatrix} -s_\theta \\ s_\phi c_\theta \\ c_\phi c_\theta \end{Bmatrix} \tag{40}$$

2. Body Aerodynamic Forces and Moments

The aerodynamic forces on the projectile are split into standard steady (SA) and Magnus (MA) terms. The Magnus forces act at the Magnus center of pressure, which is different from the center of pressure of the steady aerodynamic forces:

$$\begin{Bmatrix} X_P^A \\ Y_P^A \\ Z_P^A \end{Bmatrix} = \begin{Bmatrix} X_P^{SA} \\ Y_P^{SA} \\ Z_P^{SA} \end{Bmatrix} + \begin{Bmatrix} X_P^{MA} \\ Y_P^{MA} \\ Z_P^{MA} \end{Bmatrix} \tag{41}$$

where

$$X_P^{SA} = -\frac{\pi}{8} \rho V^2 D^2 (C_{X0} + C_{X2} \varepsilon^2) \tag{42}$$

$$Y_P^{SA} = -\frac{\pi}{8} \rho V^2 D^2 \left[C_{NA} \frac{v}{V} \right] \tag{43}$$

$$Z_P^{SA} = -\frac{\pi}{8} \rho V^2 D^2 \left[C_{NA} \frac{w}{V} \right] \tag{44}$$

$$X_P^{MA} = 0 \tag{45}$$

$$Y_P^{MA} = \frac{\pi}{8} \rho V^2 D^2 \frac{pD}{2V} \left[C_{YPA} \frac{w}{V} \right] \tag{46}$$

$$Z_P^{MA} = -\frac{\pi}{8} \rho V^2 D^2 \frac{pD}{2V} \left[C_{YPA} \frac{v}{V} \right] \tag{47}$$

The total applied body moments contain steady (SA), unsteady (UA), and Magnus (MA) terms:

$$\begin{Bmatrix} L_P^A \\ M_P^A \\ N_P^A \end{Bmatrix} = \begin{Bmatrix} L_P^{SA} \\ M_P^{SA} \\ N_P^{SA} \end{Bmatrix} + \begin{Bmatrix} L_P^{UA} \\ M_P^{UA} \\ N_P^{UA} \end{Bmatrix} + \begin{Bmatrix} L_P^{MA} \\ M_P^{MA} \\ N_P^{MA} \end{Bmatrix} \tag{48}$$

The steady body aerodynamic moment is computed with a cross product between the distance vector from the center of gravity (c.g.) to the center of pressure and the steady body aerodynamic force vector above. Likewise, the Magnus aerodynamic moment is computed with a cross product between the distance vector from the center of mass to the center of Magnus force and the Magnus force vector.

The unsteady body aerodynamic moment provides a damping source for projectile angular motion

$$L_P^{UA} = \frac{\pi}{8} \rho V^2 D^3 \left[C_{LDD} + \frac{pD}{2V} C_{LP} \right] \tag{49}$$

$$M_P^{UA} = \frac{\pi}{8} \rho V^2 D^3 \left[\frac{qD}{2V} C_{MQ} \right] \tag{50}$$

$$N_P^{UA} = \frac{\pi}{8} \rho V^2 D^3 \left[\frac{rD}{2V} C_{MQ} \right] \tag{51}$$

The above equations use the following intermediate expressions:

$$\varepsilon = \frac{\sqrt{v^2 + w^2}}{\sqrt{u^2 + v^2 + w^2}} \tag{52}$$

The aerodynamic coefficients and aerodynamic center distances are all a function of the local Mach number at the center of mass of the projectile. Computationally, these Mach number dependent parameters are obtained by a table look-up scheme using linear interpolation.

III. Results

A. Description of Projectile

The projectile used in this simulation is a representative direct fire fin-stabilized projectile with diameter of 0.0879 ft. The projectile mass, mass center measured along the station line, roll inertia, and pitch inertia are 0.344 slugs, 1.38 ft, 0.0002387 slug-ft^2, and 0.1771784 slug-ft^2, respectively. Unless otherwise specified, the ratio of the internal translating mass to the projectile mass and the cavity distance from the composite c.g. along the body x axis is 1.3% and 0.8995 ft, respectively. The line of movement of the internal translating mass is along the J_P axis of the projectile. The viscous damping coefficient for the cavity sleeve is 0.01 lbs-s/ft. In all the following cases, the projectile is traveling through a standard atmosphere without atmospheric wind. A schematic of the example projectile is shown in Fig. 2.

B. Description of Controller

To examine the amount of trajectory deflection with this control mechanism, a control law is created to move the internal mass in a prescribed manner. The control force exerted on the internal translating mass is generated by a feedback linearization controller [10] which assumes full state feedback. The equation used to compute the control force is

$$f_{input} = \frac{m_P m_T}{m} \ddot{s} + c_V \dot{s} + \gamma - m_T (\ddot{s} - \ddot{s}_{command})$$
$$- 2 m_T \xi \omega_n (\dot{s} - \dot{s}_{command}) - m_T \omega_n^2 (s - s_{command}) \tag{53}$$
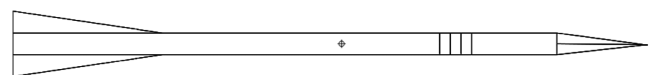

Fig. 2 Schematic of example 57-mm projectile.

where γ represents the remaining terms of the internal translating mass translational dynamic equation presented in Eq. (26). In all of the following cases, the control parameters, ξ and ω_n, are given by 1.0 and 10^7 rad/s, respectively.

C. Example Simulation

The internal moving mass projectile dynamic model was validated against a 6-degree-of-freedom simulation. Three simulations were run. The first was a nominal 6-degree-of-freedom trajectory of the projectile without the moving mass ("6DOF"). The second was a 7-degree-of-freedom trajectory with the moving mass, where the controller kept the moving mass in the center of the cavity ("7DOF centered"). The third ("7DOF oscillated") was a 7-degree-of-freedom trajectory with the moving mass, where the controller oscillated the mass exactly at the roll frequency according to

$$s_{command} = A_T \cos(\phi + \phi_T) \qquad (54)$$

where $A_T = 0.043$ ft and $\phi_T = 0$. Note that the phase angle ϕ_T determines the plane in the inertial frame in which the mass oscillates and therefore the direction in which swerve occurs. Figure 3 describes the motion of the internal translating mass at various intervals along one roll cycle for the mass-oscillated case for $\phi_T = 0$.

In all cases, the projectile initial conditions were as follows: $x = 0.0$ ft, $y = 0.0$ ft, $z = 0.0$ ft, $\phi = 90.0$ deg, $\theta = 0.573$ deg, $\psi = 0.0$ deg, $u = 5679$ ft/s, $v = 0.0$ ft/s, $w = 0.0$ ft/s, $p = 380$ rad/s, $q = 0.0$ rad/s, and $r = 0.0$ rad/s. In the 7DOF cases, the initial internal translating mass position and velocity was 0.0 ft and 0.0 ft/s, respectively, and the viscous damping coefficient of the cavity was 0.01 lbs-s/ft. Also, the moving mass was 1.3% of the projectile mass, and the cavity was placed 0.8995 ft behind the center of gravity. As demonstrated in Figs. 4–15, the trajectories for the 6DOF and mass-centered case match almost exactly, providing a validation that the 7DOF model reduces to the 6DOF model when the

Fig. 5 Cross range vs time.
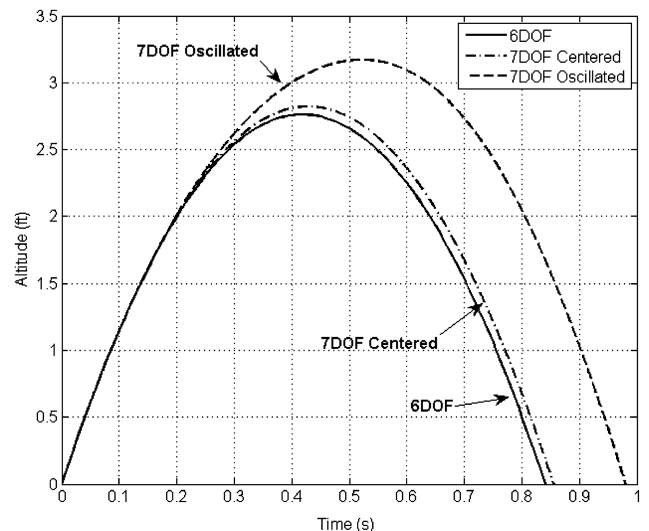
Fig. 6 Altitude vs time. Swerve in the K_I direction with $\phi_T = 0$ is an off-axis response of the spinning projectile.

Fig. 3 Moving mass position, velocity (v), and acceleration (a) over one roll cycle for $\phi_T = 0$. Mass motion is sinusoidal and has the same frequency as the projectile roll rate.
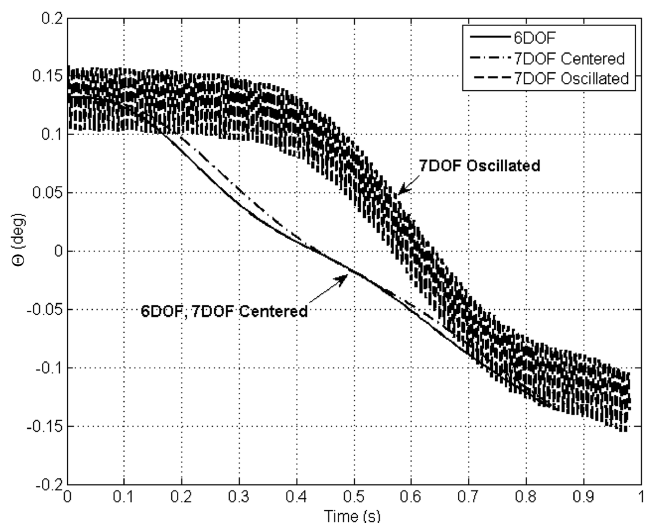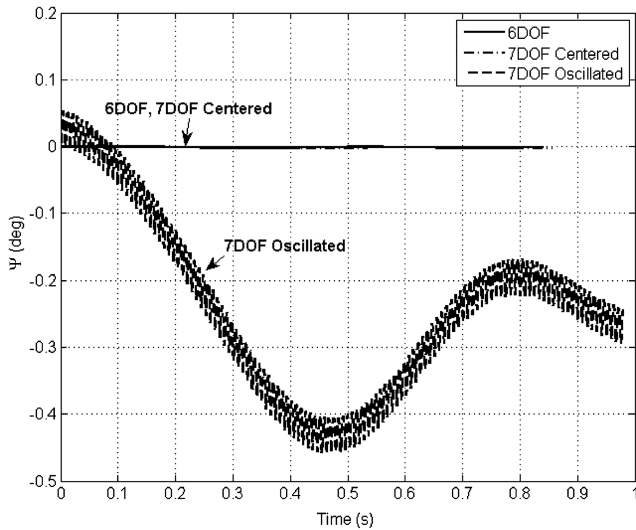

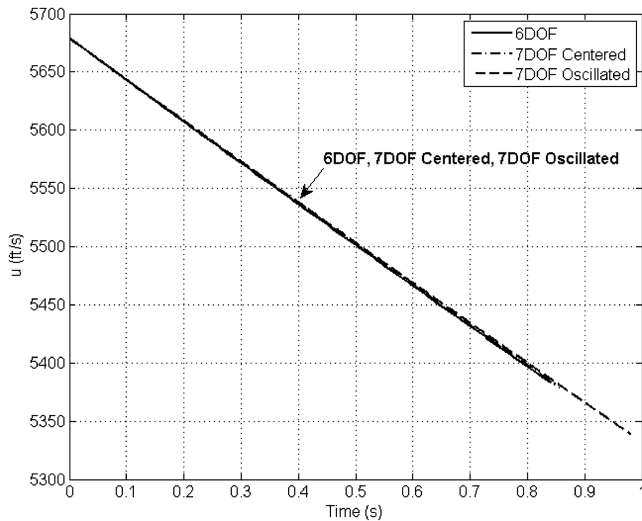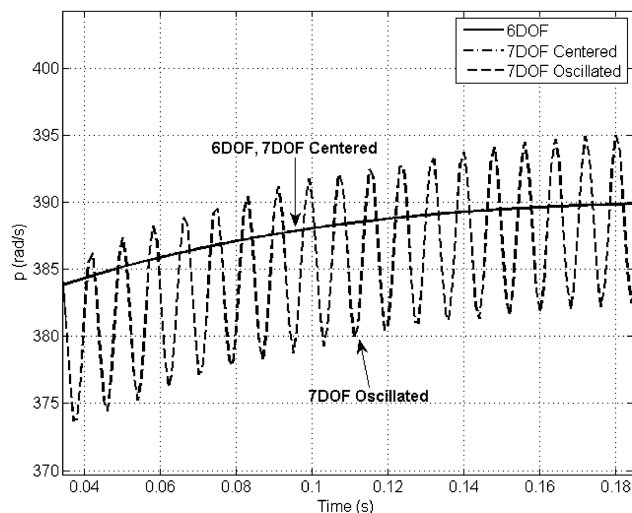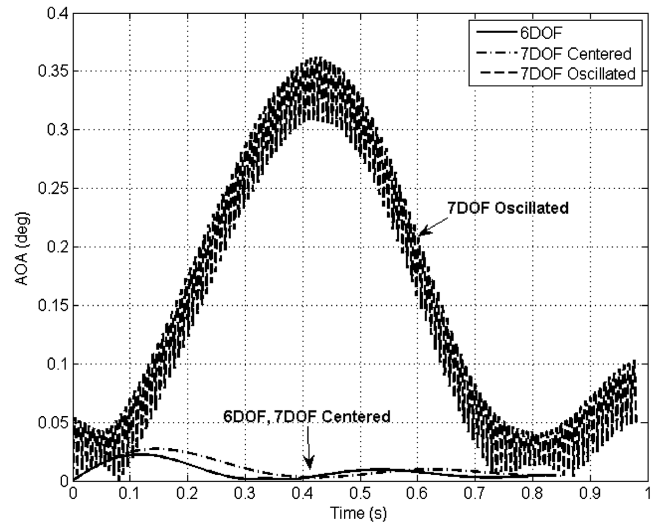Fig. 4 Range vs time.

Fig. 7 Body pitch attitude vs time.

Fig. 8　Yaw angle vs time.

Fig. 11　Angle of attack vs time. This figure demonstrates that the net moment over each spin revolution caused by internal translating mass motion causes angle of attack perturbations, which in turn lead to swerve. These angle of attack variations contrast sharply with the relatively steady angle of attack of the 6DOF trajectory.

internal mass is held fixed. Also, note that by vibrating the internal mass at the roll frequency significant cross range is created.

Average power required over the trajectory for the mass-oscillated case was 0.6082 Hp, and maximum power required was 1.0071 Hp. The magnitude of the power required and the force exerted by the controller decreased slightly corresponding with the slight decrease in projectile roll rate over the mass-oscillated trajectory.

Fig. 9　u vs time.

D.　Control Authority Analysis

Several trade studies were run to examine the control authority of the moving mass projectile. In all of the following trade studies, shown in Figs. 17–28, the projectile initial conditions were as follows:　$x = 0.0$ ft,　$y = 0.0$ ft,　$z = 0.0$ ft,　$\phi = 90.0$ deg, $\theta = 0.0$ deg,　$\psi = 0.0$ deg,　$u = 5679$ ft/s,　$v = 0.0$ ft/s,　$w = 0.0$ ft/s,　$q = 0.0$ rad/s, and　$r = 0.0$ rad/s. Total swerve values are reported at a range of 5000 ft for all trade studies shown.

Figure 16 shows total swerve as a function of the frequency of internal mass oscillation. Swerve is maximized when the input frequency of the internal mass is locked to the spin rate of the projectile. Furthermore, although not shown on a plot, swerve caused by holding the mass at the end of the cavity with spin rate set to zero

Fig. 10　p vs time.
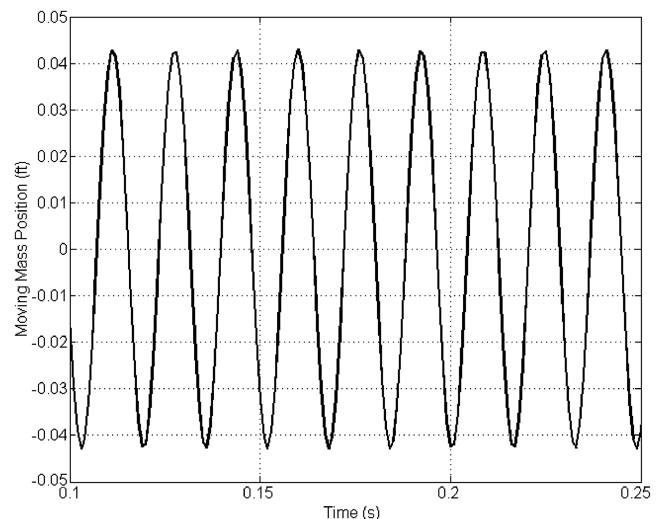
Fig. 12　Translating mass position vs time for nine roll cycles.

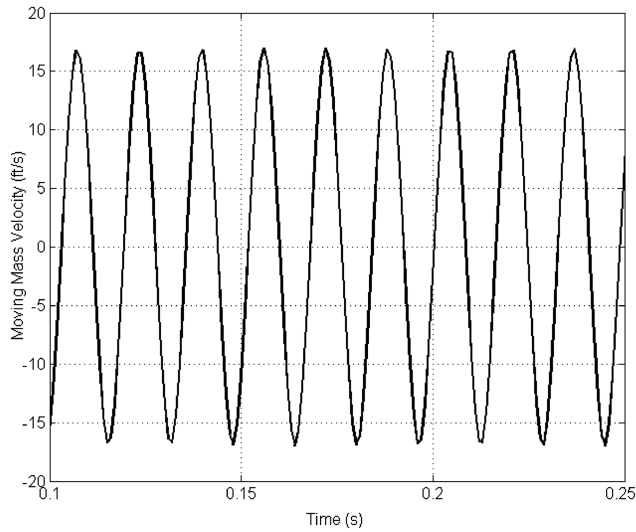**Fig. 13   Translating mass velocity vs time for nine roll cycles.**
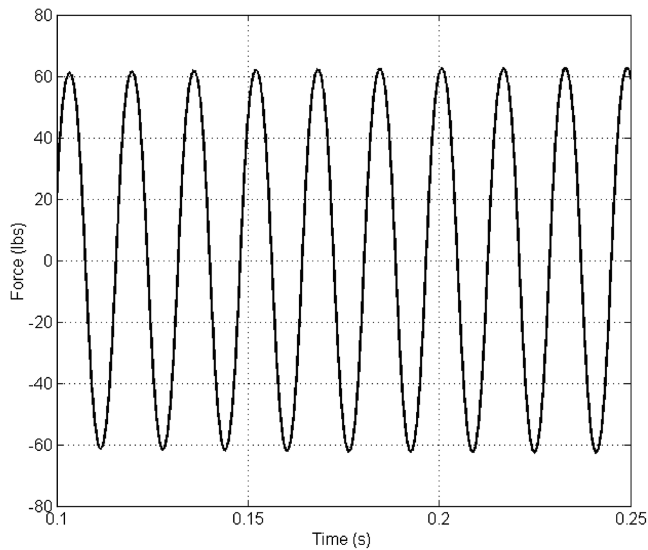

Fig. 14   Force vs time for the mass-oscillated case for the nine roll cycles.
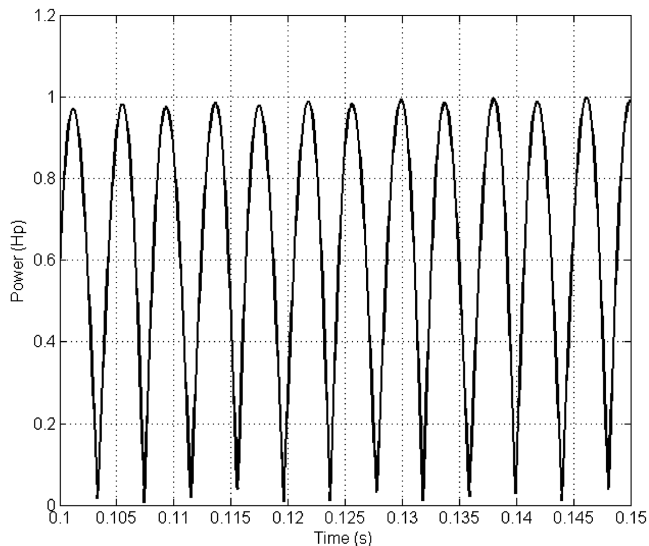

Fig. 15   Power vs time for the mass-oscillated case for the selected time interval.
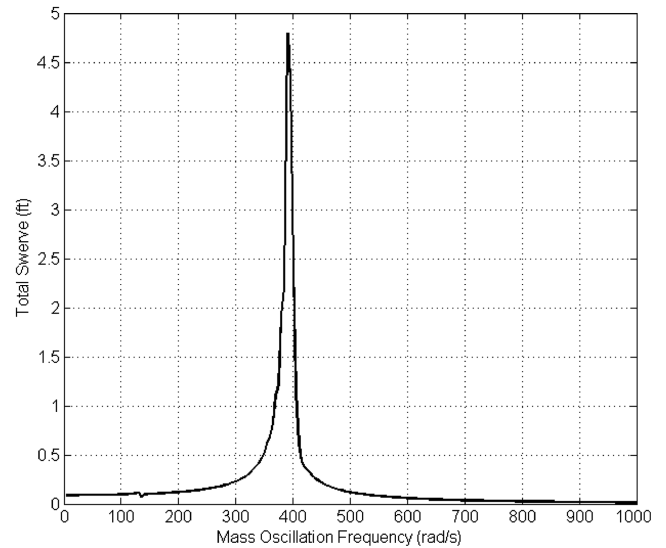

Fig. 16   Input frequency vs swerve for the spinning projectile. Total swerve is measured over 5000 ft. Harmonics of the roll frequency show no swerve response. It should be noted that control authority suffers in the above cases due to the fact that the mass oscillation frequency is not locked to the spin. Furthermore, projectile spin decays over 5000 ft and therefore the peak is around the initial roll rate of 380 rad/s is slightly spread.
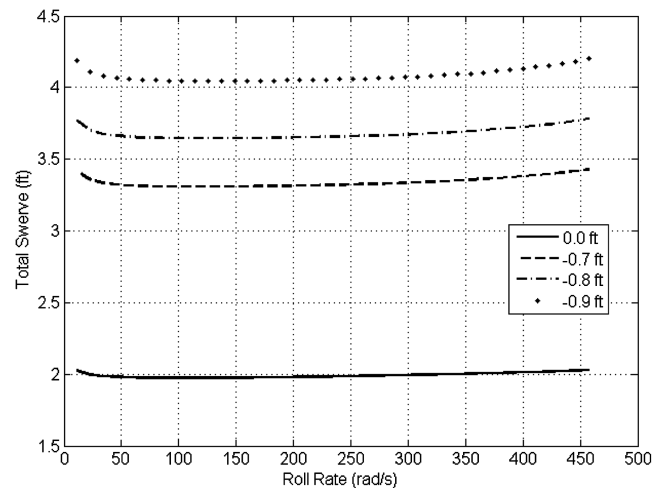
Fig. 17   Total swerve vs projectile roll rate for various cavity offsets (r_{PA}). An increased offset from the cavity to the c.g. results in greater control authority. When the cavity is placed at the c.g., less swerve results as would be predicted.

yields nearly negligible swerve leading to the conclusion that this control mechanism is not driven by a drag-induced moment from mass center offset but rather by a dynamic coupling between the projectile body and the internal mass. This coupling leads to angular perturbations to the projectile, which leads to aerodynamic angle of attack, which leads to normal force and subsequent swerve.

Based on the observation that maximum swerve can be achieved by locking the input frequency of the mass oscillation to the projectile roll rate, the average control moment for spin revolution can be obtained analytically. Assuming the translating mass oscillates according to

$$s = A_T \cos(\phi + \phi_T) \tag{55}$$

and that the cavity is aligned with the J_P axis, the moment equation given in Eq. (32) can be solved to find the approximate average control moment in the J_{NR} and K_{NR} directions,
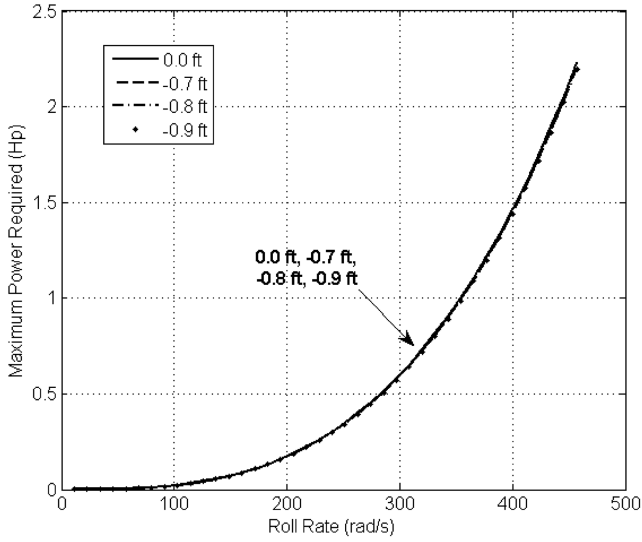
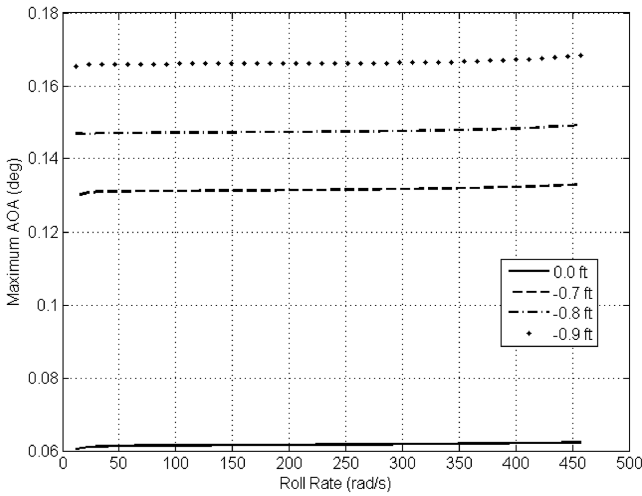Fig. 18 Maximum power required vs projectile roll rate for various cavity offsets.
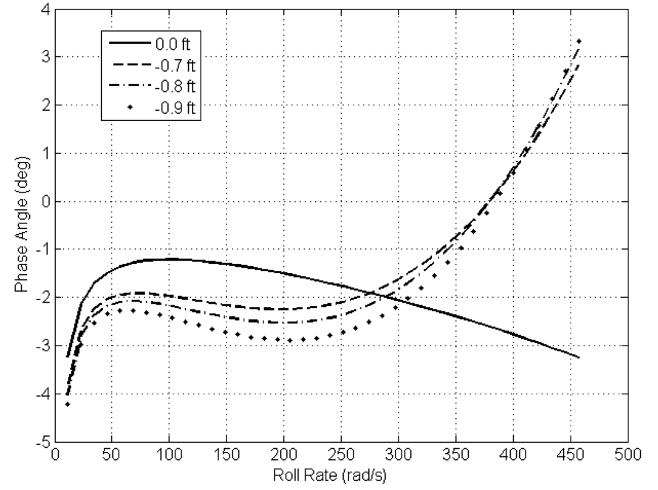

Fig. 20 Phase angle of swerve vs projectile roll rate for various cavity offsets.

following trade study, r_{PA} was varied between 0 and 0.9 ft behind the c.g., where the case of 0-ft offset represents a cavity at the projectile c.g. The mass was oscillated at the corresponding roll frequency. Also, note that the phase angle of the swerve is defined at the impact point as

$$\Phi_I = \tan^{-1}\left(\frac{\Delta z_S}{\Delta y_S}\right) \qquad (58)$$

An interesting aspect of this result is that more control authority can be gained from a cavity farther from the c.g. at a lower spin rate. This provides a way to increase control authority without the prohibitive increases in force and power required resulting from high spin rates.

The mass ratio of the internal translating mass to the projectile mass also has a significant effect on control authority. A larger mass ratio gives rise to more dynamic coupling between the mass oscillation and the body roll rate. Figure 21 shows that, for equivalent roll rates, a heavier internal mass produces noticeable improvements in control authority. The following trade study considers the projectile with $r_{PA} = 0.8995$ ft and a variable mass ratio.

Although increased mass percentage increases the control performance, the heavier mass requires higher power consumption to oscillate the mass, especially at increased roll rates.
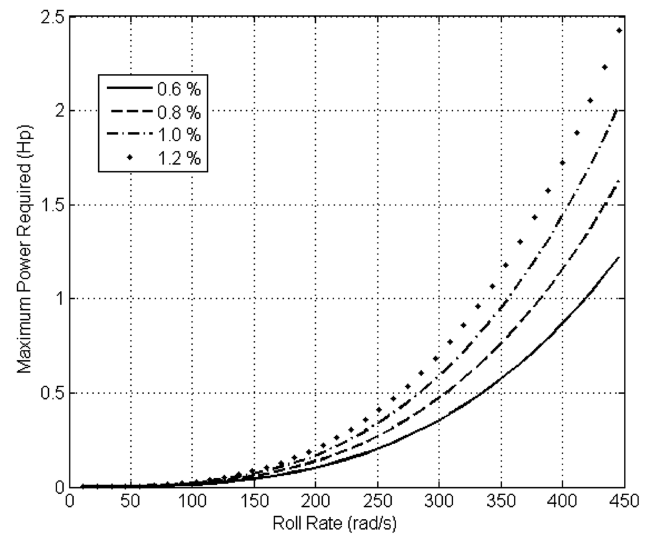

Fig. 19 Maximum angle of attack vs projectile roll rate for various cavity offsets.

$$M_{JNR} = \frac{m_P m_T}{m}\left(-\frac{1}{2}A_T x_T \tilde{q}\,\tilde{r}\cos(\phi_T) + \frac{1}{2}A_T x_T \tilde{r}^2 \sin(\phi_T)\right.$$
$$\left. + \dot{\tilde{q}}\left(x_T^2 + \frac{1}{4}A_T^2\sin^2(\phi_T) + \frac{1}{8}A_T^2\right)\right)$$
$$+ \frac{m_P m_T}{m}\left(\frac{1}{4}A_T^2\dot{\tilde{r}}\sin(\phi_T)\cos(\phi_T) + \frac{1}{2}A_T^2\tilde{p}\,\tilde{r}\right) \qquad (56)$$

$$M_{KNR} = \frac{m_P m_T}{m}\left(-\frac{1}{2}A_T x_T \tilde{q}\,\tilde{r}\sin(\phi_T) + \frac{1}{2}A_T x_T \tilde{q}^2 \sin(\phi_T)\right.$$
$$\left. + \dot{\tilde{r}}\left(x_T^2 + \frac{1}{4}A_T^2\cos^2(\phi_T) + \frac{1}{8}A_T^2\right)\right)$$
$$+ \frac{m_P m_T}{m}\left(\frac{1}{4}A_T^2\dot{\tilde{q}}\sin(\phi_T)\cos(\phi_T) - \frac{1}{2}A_T^2\tilde{p}\,\tilde{q}\right) \qquad (57)$$

The above expressions demonstrate there is a net control moment dependent on all angular velocities as well as mass oscillation amplitude, the cavity offset, and the internal translating mass size.

Increasing the cavity distance from the projectile center of gravity, depicted as r_{PA} in Fig. 1, serves to increase control authority. In the

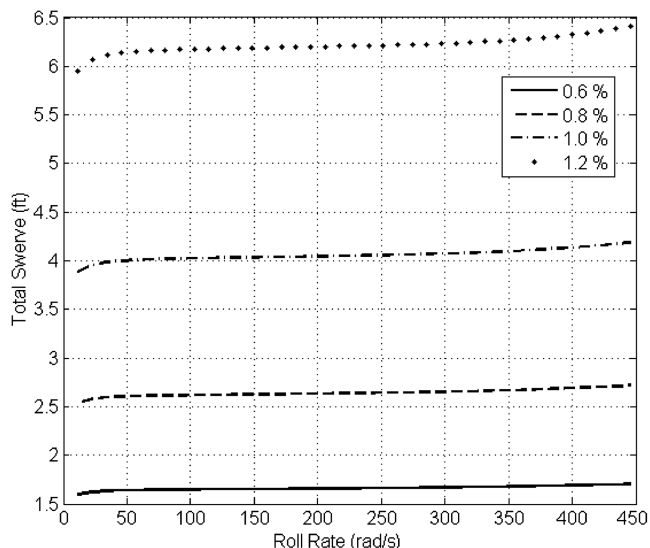Fig. 21 Maximum power required vs projectile roll rate for various mass sizes.

Fig. 22 Swerve vs projectile roll rate for various mass sizes. A 1% mass ratio signifies that the internal translating mass is 1% of the mass of the projectile without the cavity.
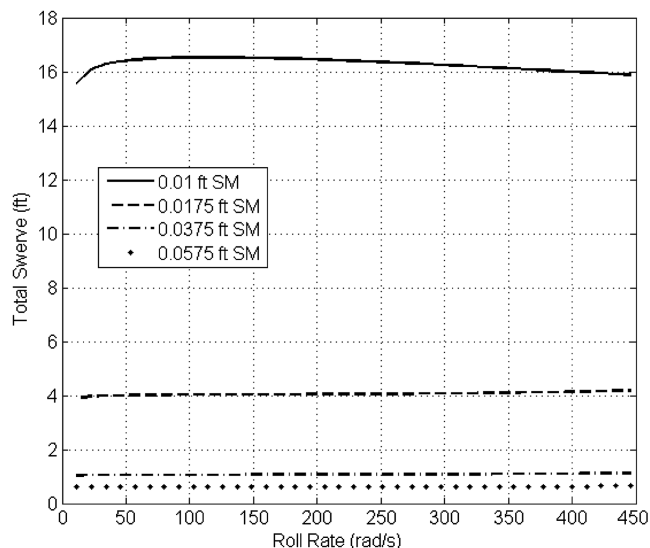

Fig. 23 Maximum angle of attack vs projectile roll rate for various mass sizes.
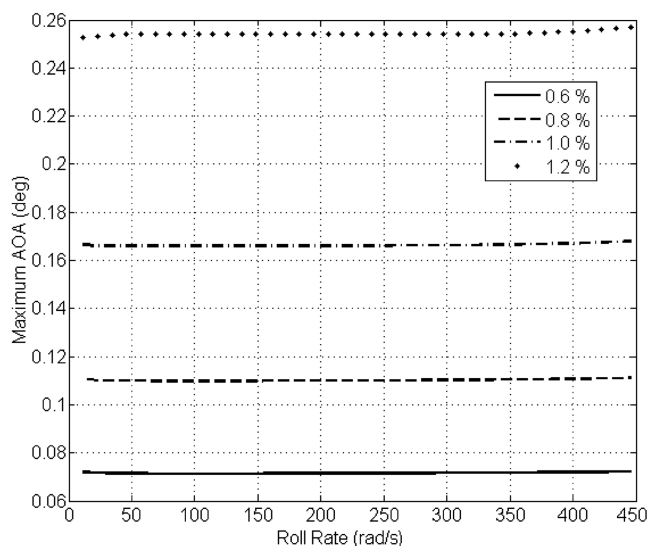
Fig. 24 Phase angle of swerve vs projectile roll rate for various mass sizes.

Fig. 25 Swerve vs projectile roll rate for reduced-stability projectile.
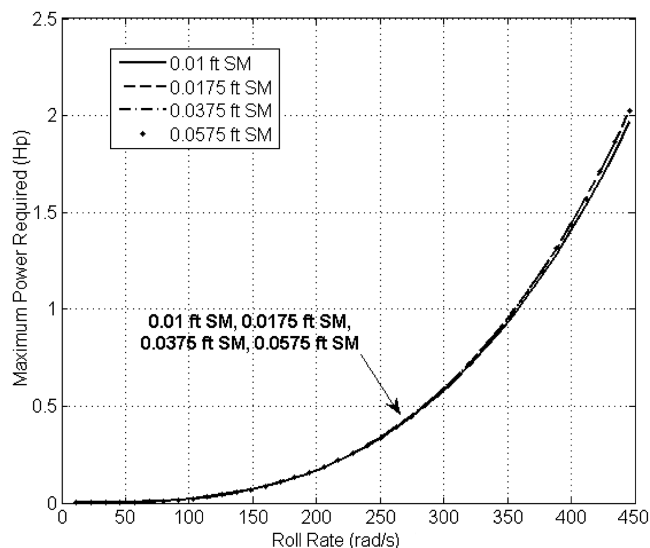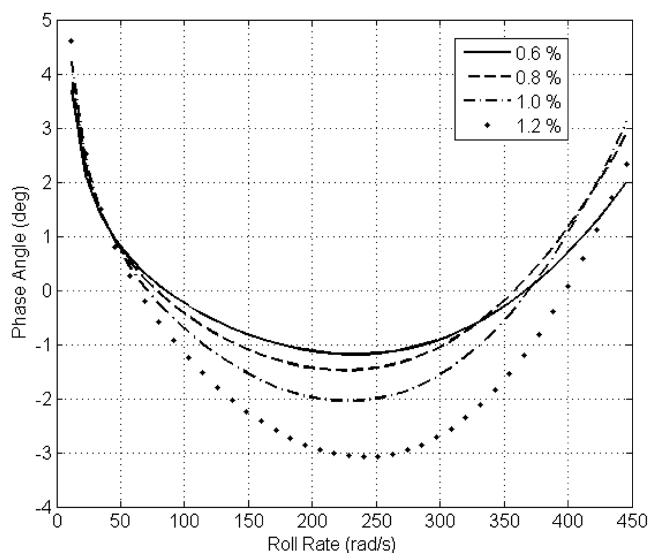

Fig. 26 Maximum power required vs projectile roll rate for reduced-stability projectile.
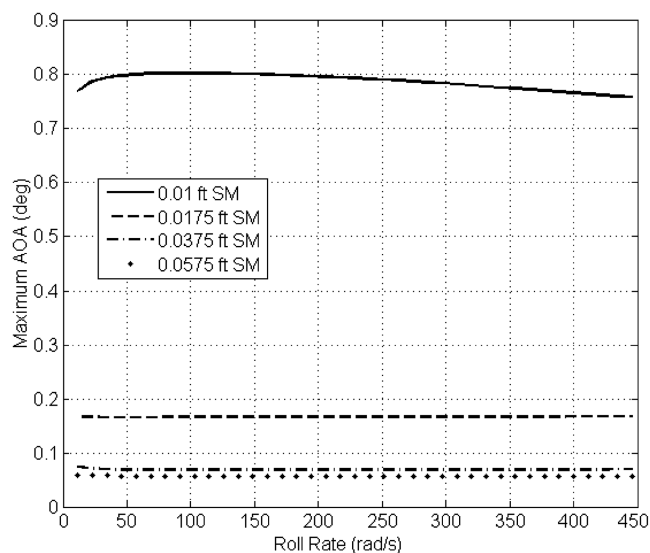

Fig. 27 Maximum angle of attack vs projectile roll rate for reduced-stability projectile.
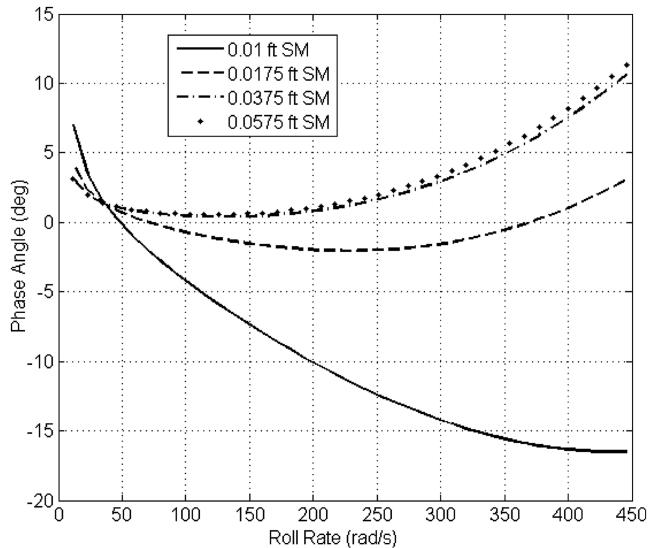
Fig. 28   Phase angle of swerve vs projectile roll rate for reduced-stability projectile.

A trade study examined the control authority in response to reduced static stability of the projectile. The nominal projectile is statically stable with a static margin of approximately 0.49 ft. Decreasing the magnitude of the static margin caused increased control authority, although at low spin rates some reduced-stability rounds experienced excessively high angles of attack. The following trade study considered a projectile with variable static margin, a 1.0% mass ratio, and $r_{PA} = 0.8995$ ft.

IV.   Conclusions

The results presented here demonstrate that the internal translating mass mechanism can produce significant control authority for smart weapons applications. The projectile swerve is caused not by drag effects due to an offset center of gravity, but rather by dynamic coupling between the oscillating mass and projectile spin. These conclusions were drawn from an exhaustive set of dynamic simulations that employ a 7-degree-of-freedom model which includes motion of the projectile and internal mass. Parametric trade studies show that control authority can be significantly increased with increased roll rate, increased internal mass, increased cavity offset distance, and reduced static margin. Actuator force and power requirements increase as roll rate and internal mass increases but are insensitive to changes in cavity offset distance and projectile static margin.

References

[1] Murphy, C., "Symmetric Missile Dynamic Instabilities," *Journal of Guidance and Control*, Vol. 4, No. 5, 1981, pp. 464–471.

[2] Soper, W., "Projectile Instability Produced by Internal Friction," *AIAA Journal*, Vol. 16, No. 1, 1978, pp. 8–11.

[3] Murphy, C., "Influence of Moving Internal Parts on Angular Motion of Spinning Projectiles," *Journal of Guidance and Control*, Vol. 1, No. 2, 1978, pp. 117–122.

[4] D'Amico, W., "Comparison of Theory and Experiment for Moments Induced by Loose Internal Parts," *Journal of Guidance and Control*, Vol. 10, No. 1, 1987, pp. 14–19.

[5] Hodapp, A., "Passive Means for Stabilizing Projectiles with Partially Restrained Internal Members," *Journal of Guidance and Control*, Vol. 12, No. 2, 1989, pp. 135–139.

[6] Petsopoulos, T., Regan, F., and Barlow, J., "Moving Mass Roll Control System for Fixed-Trim Re-Entry Vehicle," *Journal of Spacecraft and Rockets*, Vol. 33, No. 1, 1996, pp. 54–61.

[7] Robinett, R., Sturgis, B., and Kerr, S., "Moving Mass Trim Control for Aerospace Vehicles," *Journal of Guidance, Control, and Dynamics*, Vol. 19, No. 5, 1996, pp. 1064–1071.

[8] Menon, P., Sweriduk, G., Ohlmeyer, E., and Malyevac, D., "Integrated Guidance and Control of Moving Mass Actuated Kinetic Warheads," *Journal of Guidance, Control, and Dynamics*, Vol. 27, No. 1, 2004, pp. 118–127.

[9] Frost, G., and Costello, M., "Linear Theory of a Projectile with a Rotating Internal Part in Atmospheric Flight," *Journal of Guidance, Control, and Dynamics*, Vol. 27, No. 5, 2004, pp. 898–906.

[10] Frost, G., and Costello, M., "Control Authority of a Projectile Equipped with an Internal Unbalanced Part," *Journal of Dynamic Systems, Measurement, and Control*, Vol. 128, No. 4, 2006, pp. 1005–1012. doi:10.1115/1.2363205